Determining the geometric surface area of mesoporous materials

Yijie Wang
Tsinghua University
Zhixin Chen
Tsinghua University
Liming HU (gehu@tsinghua.edu.cn)
Tsinghua University https://orcid.org/0000-0001-8522-9864

Article

Keywords:

Posted Date: September 12th, 2022

DOI: https://doi.org/10.21203/rs.3.rs-2018509/v1

Determining the geometric surface area of mesoporous materials

Yijie Wang[1], Zhixin Chen[1], and Liming Hu[1]*

Submitted to *Nature Communications*

09/01/2022

[1]State Key Laboratory of Hydro-Science and Engineering, Dept. of Hydraulic Engineering, Tsinghua University, Beijing 100084, China

*Corresponding author: gehu@tsinghua.edu.cn

Abstract:

Specific surface area is an important property of porous materials and mainly measured using nitrogen isotherm and Brunauer–Emmett-Teller (BET) equation. BET surface area is remarkably higher than geometric surface area, which is defined as the surface area of the crystal geometry structure. However, many studies directly use the BET surface area as the geometric surface area. We proposed a simple, general, and accurate method that only needs nitrogen adsorption isotherm as input to calculate the geometric surface area of mesoporous materials using an iterative algorithm. The proposed method considers the adsorbent influences combined with the physical state of adsorbed nitrogen in estimating the surface area. We utilized 18 isotherms generated by molecular simulations and actual experiments to cover a wide range of materials, including catalysts, minerals, and carbon-based tube, and validate the effectiveness of the proposed method. Our results showed that the surface area determined by the proposed method and referenced geometric area are almost identical. The surface obtained by the proposed method can be typically considered a geometric surface area.

Specific surface area is an important property that can characterize porous materials and intrinsically affect the practical performance of many porous materials, such as catalysts[1], minerals[2], and carbon nanotubes[3]. Gas adsorption has been widely used to measure the surface area, among which measurements utilizing nitrogen as the adsorbate at 77 K is the most common because of its stability and accessibility[4]. The measured nitrogen isotherm is analyzed through the Brunauer–Emmett-Teller (BET) equation (Method) to evaluate the monolayer adsorption capacity m_m in the traditional method[5]. The surface area is calculated as follows:

$$S_{BET} = m_m N_A \sigma_0 / M_{N2}, \quad (1)$$

where S_{BET} is the calculated BET surface area (m^2/g), M_{N2} is the molar weight of nitrogen, N_A is the Avogadro number, and σ_0 is the cross-sectional area of nitrogen. The cross-sectional area of nitrogen is critical in achieving a meaningful value of the BET surface area. The typically used value of the cross-sectional area of nitrogen is 16.2 $Å^2$, which is also set as the default value in the majority of commercial software programs. However, the surface area is highly overestimated by the nitrogen isotherm-based BET analysis[6,7].

A noncontroversial standard reference value of surface area is necessary to assess the accuracy of the BET surface area. The geometric surface area of the material crystal structure is a reliable value and considered the true surface area in some studies[8]. The geometric surface area of adsorbent can be clearly and easily calculated in computer simulations, such as grand canonical Monte Carlo (GCMC) simulations[7], however it is difficult to measure in experiments. The BET analysis result of argon at 88 K is regarded as a satisfactory approximation to the geometric surface area[8] because argon is insensitive to solid surface properties and the state of adsorbed argon alters slightly from the bulk liquid state. However, the traditional BET method chooses nitrogen as the common adsorbate given that liquid argon is remarkably less assessable than liquid nitrogen. Many

studies use the BET surface area obtained from the traditional method as the geometric surface area due to the measuring limitation. Overestimating the surface area in a similar proportion exerts a minimal effect in some studies. However, the absolute value of the geometric surface area is very important in other studies. For example, the geometric surface area is required in the preparation of supported catalyst with a certain monolayer loading of active species[9]. In order to assess the quality of the sample metal–organic frameworks (MOFs), the experimentally determined surface area is often compared with the geometric surface area, which is calculated from the theoretical MOF crystal[10]. Moreover, the value of the geometric surface area is generally used as an important parameter in various models of many disciplines, such as the model for calculating bound water in soil[11-13].

The following may cause overestimation in the traditional BET method when the geometric surface area is used as the reference. First, the BET equation becomes invalid once micropore (pore width < 2 nm) filling occurs[14]. Second, the cross-section area σ_0 used for surface area calculation presents an improper value. The BET equation is theoretically derived from the adsorption phenomenon occurring on a plane[5]. Complex adsorption and capillary condensation taking place in micropores[15,16] are beyond the scope of BET. If the mesoporous material with a pore width between 2 and 50 nm, which is also the range of a large number of significant materials and suitable for the test procedure of classical BET analysis, is considered, then the cross-sectional area of nitrogen σ_0 becomes the principal reason for overestimation. The widely used σ_0 value of 16.2 $Å^2$ is provided by the density of liquid nitrogen at 77 K and 0.1 MPa and far from the actual adsorbed phase, especially for the adsorbed first layer. The nitrogen molecule presents a quadrupolar moment and can interact with a hydroxylated solid surface that causes dense packing on the surface. The dense packing of adsorbed nitrogen is highly dependent on solid surface

properties. Hence, the appropriate cross-section area is different for different materials, and diverse cross-section area values are provided to eliminate the discrepancy between BET and geometric surface areas[17,18].

A universal method for calculating geometric surface area from isotherm is still lacking. We put forward a simple and general method to determine the geometrical surface area using the nitrogen adsorption isotherm of the sample. The proposed method combined the thermodynamic equilibrium between adsorbed and gas phases of nitrogen and the physical state equation of nitrogen to estimate the average density of the adsorbed layer. The final surface area result was determined through the average density of monolayer and monolayer adsorption capacity m_m from classical BET analysis. This study focuses on mesoporous materials due to the scope of traditional BET analysis. Two sets of isotherm data were adopted to validate the proposed method, in which one was generated via GCMC simulations to utilize the advantage of GCMC in calculating the geometric surface area, and the other was the actual measured data. The BET analysis results of argon for the same samples at 88 K were selected as the reference value of the geometric surface area. The validation process covered a wide range of materials including silica, aluminosilicates, clay minerals, and carbon-based pores.

Results

Thermodynamic equilibrium in the adsorbate-adsorbent system

The total potential of gas nitrogen is equal to the total potential of adsorbed nitrogen at thermodynamic equilibrium. The nitrogen isotherm describes the equilibrium, that is, the relationship between nitrogen gas pressure and adsorbed nitrogen amount (Fig. 1a). The horizontal axis of isotherms is generally expressed as the ratio of environmental gas pressure to saturated nitrogen vapor pressure at 77 K. Meanwhile, the vertical axis is expressed as the mass of adsorbed nitrogen per gram of adsorbent. The total potential ψ (MPa or J/m^3) of gas nitrogen can be calculated on the basis of the bulk liquid nitrogen at 77 K and 0.1 MPa using Kelvin's equation[19,20]

$$\psi = RT / v_{\mathrm{m}} \ln(p / p_0), \quad (2)$$

where R is the gas constant; T is 77 K; v_{m} is the molar volume of bulk liquid nitrogen; p is the equilibrium gas pressure; and p_0 is the saturated vapor pressure of nitrogen (0.1 MPa). Fig. 1a shows the one-to-one correspondence of gas pressure and total potential. Nitrogen is a probe molecule in a gas adsorption experiment that can interact with the adsorbent surface and be adsorbed. Strong interactions between nitrogen and the surface correspond to the tight adsorption of nitrogen cumulates, thereby indicating a high internal pressure (p_{ad}) within the adsorbed molecules. The total potential can also be derived from the state of adsorbed nitrogen due to the equilibrium between gas and adsorbed phase. The interaction energy between the adsorbent and adsorbate molecule is labeled as the adsorptive potential ψ_{ad}. Referring to the bulk liquid nitrogen under p_0, the total potential of adsorbed nitrogen is expressed as[21]

$$\psi = \psi_{\mathrm{ad}} + p_{\mathrm{ad}} - p_0. \quad (3)$$

Notably, we use the same symbol ψ because the total potentials of adsorbed and gas phases are equal at equilibrium.

123 As shown in Fig. 1b, the adsorption of the adsorbent triggers the condensation of nitrogen
124 molecules even at a gas pressure lower than saturation. The adsorption phenomenon originates
125 from the intermolecular and surface forces, which decay remarkably with the increase of spatial
126 distance [22]. The nature of adsorptive potential (generally negative and reaches zero at infinity,
127 Fig. 1c) affects the pressure p_{ad} within the adsorbed phase body. The closer to the adsorbent surface,
128 the higher p_{ad}, as shown in Figs. 1b and 1d. In addition to the energy equilibrium, a mechanical
129 equilibrium also exists at the interface between adsorbed and gas phases, that is, $p_{ad}(h) = p$, where
130 h is the thickness of the adsorbed film (Fig. 1b). The variation of p_{ad} illustrates its function as the
131 spatial distance to the adsorbent surface.
132 The mass of adsorbed phase rises and the adsorbed film gradually thickens as the gas pressure
133 p rises. However, the mechanical equilibrium at the liquid–gas (adsorbed phase–gas) interface is
134 always workable, as shown in Fig. 1d. Eqs. 1 and 2 demonstrated that the adsorptive potential at
135 location h can be calculated using gas pressure p. Hence, the variation of adsorptive potential with
136 space can be obtained from the connection between the rising pressure and the changing thickness
137 of the adsorbed film. The following simple scaling law can be used to determine the film
138 thickness[23]:
139 $$m = S \times h \times \rho^{ave}, \quad (4)$$
140 where m is the adsorbed mass (g/g), S is the geometric surface area of the adsorbent, and ρ^{ave} is the
141 average density of the adsorbed film (g/cm^3). As mentioned above, high and nonuniform pressure
142 within the adsorbed phase caused by adsorption further leads to the increase in the average density
143 of adsorbed phase. Studies have typically used the pressure–density relationship of liquid nitrogen
144 at 77 K[19,24].

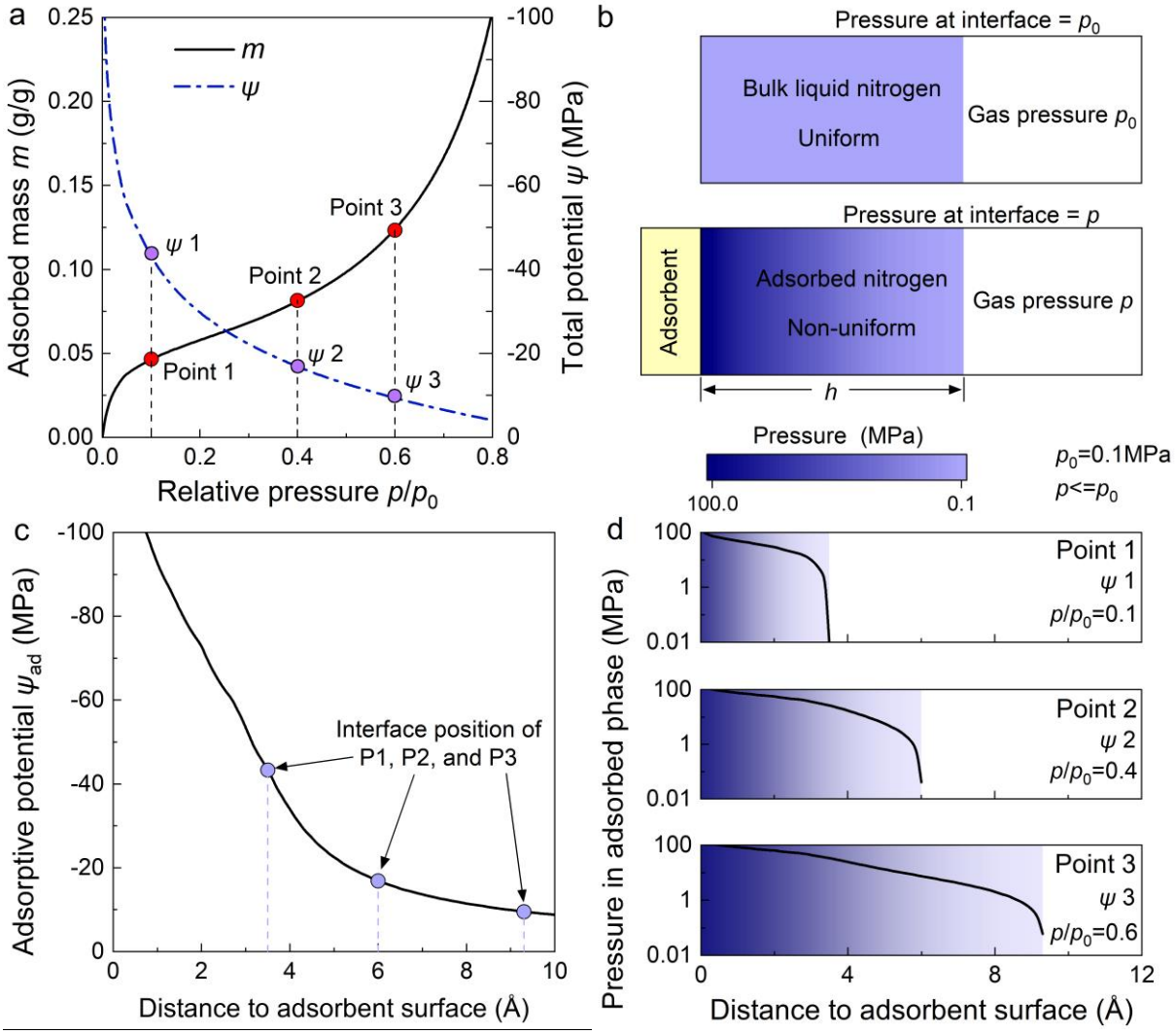

Fig. 1 Illustration of thermodynamic analysis. a Generic nitrogen adsorption isotherm and the one-to-one relationship between gas pressure p and total potential ψ. **b** Comparison of bulk liquid nitrogen and adsorbed nitrogen, where h is the adsorbed film thickness. **c** Illustration of adsorptive potential, which decays with the spatial distance to the adsorbent surface. **d** Illustration of pressure distribution changes in the adsorbed phase at different gas pressure values (total potential).

Gas pressure p, adsorptive potential ψ_{ad}, local pressure within the adsorbed layer p_{ad}, thickness h and average density ρ^{ave} of the adsorbed layer, geometric surface area S, and adsorbed mass m are all intrinsically related when the adsorbed phase and gas reach equilibrium after synthesizing Eqs. 2–4. The two ends of the chain are gas pressure p and adsorbed mass m, thereby forming the nitrogen isotherm. Utilizing the nitrogen isotherm to derive the geometric surface area

157 is rational and sufficient because the nitrogen isotherm is the macrocosmic manifestation of the
158 nitrogen–adsorbent interaction.
159
160 **Working path of the calculation of the geometric surface area**
161 Surface area *S* connects the adsorbed mass macroscopically and the adsorbed film properties
162 microscopically, as shown in Eq. 4. The adsorbed film properties, including thickness and average
163 density of adsorbed film, are directly controlled by the adsorptive potential. Therefore, determining
164 the adsorptive potential first is necessary to obtain the *S* value. As shown in Figs. 1c and 1d, the
165 adsorptive potential and local pressure in the adsorbed phase are functions of the spatial position.
166 However, the adsorptive potential is a function of the spatial position, while the pressure in the
167 adsorbed phase also changes with the gas pressure, thereby increasing the difficulty in obtaining
168 the solution. Therefore, we develop an iteration algorithm that only requires the use of nitrogen
169 isotherm as the input to solve this problem, determine the adsorptive potential, and calculate the
170 geometric surface area further.

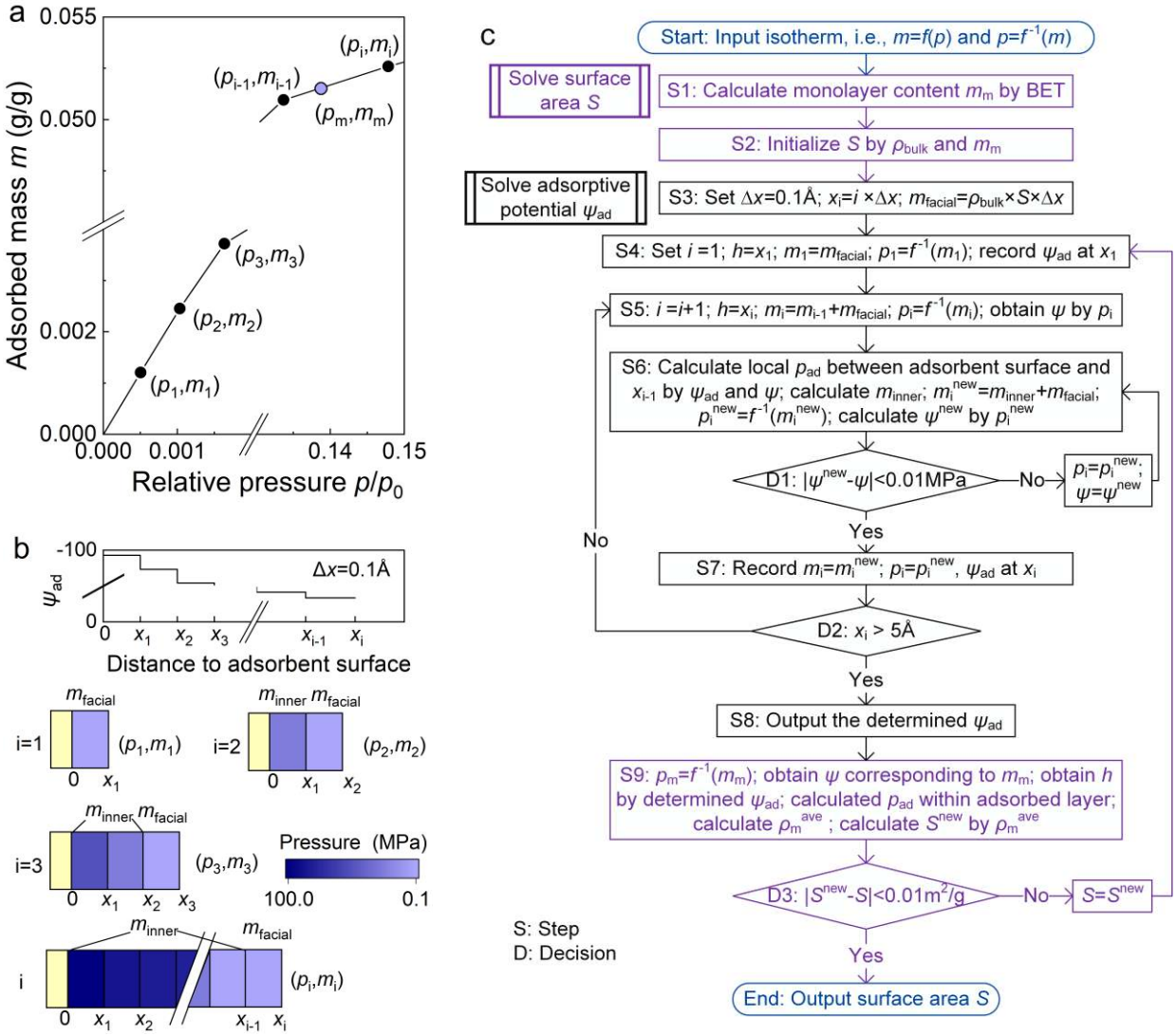

Fig. 2 Working path for the algorithm of surface area determination. a Diagram of the adsorbed mass and gas pressure corresponding to each space step in the algorithm. **b** Illustration of the pressure distribution changes with the increasing steps of the algorithm. **c** Algorithm flow details.

The determination of the adsorptive potential ψ_{ad} is based on Eqs. 2 and 3. Assuming that the location of the adsorbed phase–gas interface is x_i, then the thickness of the adsorbed film is $h = x_i$, the corresponding adsorbed mass is m_i, and gas pressure is p_i. The adsorptive potential ψ_{ad} at x_i can be expressed as follows:

$$\psi_{ad}(x_i) = RT / v_m \ln(p_i / p_0) - p_i + p_0 \quad (5)$$

182 We assume that the change of spatial position x_i is discrete and ψ_{ad} is invariant in x_{i-1} to x_i to
183 simplify the solution process. Therefore, ψ_{ad} can be solved step by step at an arbitrary spatial
184 location within the adsorption phase. The pressure distribution within the adsorbed phase at an
185 arbitrary gas pressure (or total potential ψ) can be easily calculated using Eq. 3 once ψ_{ad} is
186 determined. The average density of the adsorbed phase can then be obtained through the weighted
187 average according to the pressure–density relationship of liquid nitrogen (Method, Eq. 8), and the
188 mass of adsorbed phase can be obtained using Eq. 4. Figs. 2a and 2b show the points on the
189 isotherm corresponding to different adsorbed film thicknesses. The growth interval of the adsorbed
190 film thickness in the adsorption process is constant (Δx=0.1 Å). If we calculate the adsorbed mass
191 m_i step by step until $m_i > m_m$ (Fig. 2a), then the average density of the adsorbed phase under the
192 monolayer loading state ρ_m^{ave} can be obtained through interpolation. Therefore, the following
193 equation can be used to calculate the surface area inversely[25]:

194 $$S = m_m \times \left[N_A / M / \left(\rho_m^{ave} \right)^2 \right]^{\frac{1}{3}} \quad (6)$$

195 The inversely calculated S (Eq. 6) should theoretically be equal to the S used in the scaling law
196 (Eq. 4). This feature is a foundational decision condition in our proposed iteration algorithm.
197 The flow details of the algorithm are illustrated in Fig. 2c. The algorithm requires an isotherm
198 as the input at the start stage to indicate the functional relationship between adsorbed mass m and
199 gas pressure p. Traditional BET analysis is performed in Step 1 to calculate the monolayer content
200 m_m. The initial surface area is calculated in Step 2 using Eq. 6 with bulk liquid nitrogen density.
201 In Step 3, the algorithm begins to solve adsorptive potential ψ_{ad}. We set the spatial increment to
202 0.1 Å. Note that we always set the density within the thickness of 0.1 Å on the outer face as the
203 density of bulk liquid nitrogen ρ_{bulk} and neglect the very weak influence on liquid density caused
204 by the difference between gas and saturated gas pressures because the pressure on the outer face

of the adsorbed layer is equal to gas pressure. The mass of the small block is marked m_{facial} and the mass of the remainder adsorbed phase is marked m_{inner} in subsequent calculations, as shown in Fig. 2b. ψ_{ad} at x_1 is determined in Step 4. m_1 equals m_{facial} because m_{inner} is 0 in this step. Obtaining p_1 from the isotherm, ψ_{ad} at x_1 is easily obtained using Eq. 5. The algorithm begins to calculate ψ_{ad} at other locations in Step 5. If the spatial position changes from x_{i-1} to x_i (the adsorbed film also thickens), then the increment of m_{inner} is unknown. Hence, we use Steps 5 and 6 to determine the variation of m_{inner} iteratively. We calculate and record ψ_{ad} at this location (Step 7) once the output condition is met (Decision 1 in Fig. 2c). Move to the next location, that is, go back to Step 5. We calculate to a maximum of 5 Å (Decision 2), which is significantly more than the size of a single nitrogen molecule (roughly 3 Å). Calculate the average density of the adsorbed film corresponding to the monolayer loading using the determined ψ_{ad} combined with the monolayer content m_m from BET in Step 9. Inversely calculate the surface area S using Eq. 6. Compare the calculated S and initially estimated S to decide whether to output the S value or go back to Step 4 and use the calculated S as the new input in Decision 3.

The adsorptive effect on the adsorbed phase can be carefully captured in the surface area calculation with the aid of the proposed algorithm. Details of equations used in the algorithm are presented in the Method section.

Validation by GCMC and experimental data

Two sets of nitrogen isotherm data are utilized to validate the accuracy and generality of the proposed method for determining the geometric surface area (Table 1). The first group consists of 8 isotherms generated via the GCMC method. The significant advantage of the GCMC method is that the standard geometric surface area of the simulated model can be calculated clearly from the

geometric configuration to provide a reference for evaluating the proposed method. The second group consists of 10 isotherms with actual measurements. We use the surface area produced by analyzing the argon isotherm measured at 88 K through the BET method as the referenced geometric surface area given the difficulty in obtaining an undisputed geometric surface area in the experiment. The weak interaction between the argon and adsorbent allows the adsorbed argon to become similar to the bulk liquid argon, thereby indicating that BET analysis on the argon isotherm is more reliable than that on the nitrogen isotherm. The two sets of nitrogen isotherm data cover a wide range of material types, including minerals, catalysts, and carbon-based pores. Isotherm data of the six minerals are self-simulated, and the other data are from published literature[7,8,26-28]. A wide range of materials and different data-generated methods were adopted to ensure the reliability and objectivity of the validation process.

All chosen samples are mesoporous materials. The pore size is controlled by the simulation model for GCMC isotherm data. As shown in Fig. 3a, the distance between the two adsorbent planes for the six self-simulated minerals is 5 nm, which is significantly larger than the size of a micropore and suitable for BET analysis. Other samples also meet the mesopore size limitation. Details of the GCMC simulation are presented in the Method section. Fig. 3b demonstrates the nitrogen isotherms from GCMC. The simulated nitrogen isotherms of different minerals are similar (all isotherms are normalized using the surface area for comparison) due to their similarity in chemical compositions. The slightly higher adsorbed mass per surface area of montmorillonite compared with that of others indicates its higher adsorption capacity. Two experimentally measured isotherms of typical clays are also demonstrated in Fig. 3b to validate the reliability of the GCMC method. The maximum relative deviation of isotherm of measured kaolin and simulated kaolinite is smaller than 15%, and of measured illite clay and simulated mica is smaller

than 16%, showing good consistency. Figs. 3c–3e show the local density distribution along the z-axis for different minerals at a relative pressure of 0.01, 0.10, 0.15, and 0.35. The concentration of nitrogen molecules only near the surface indicates the absence of capillarity. This finding is consistent with the applicable conditions of BET analysis. Two distinguishable adsorbed layers are formed on one side at a relative pressure of 0.35, while only one adsorbed layer exists at a relative pressure of 0.01. Relative pressures corresponding to the monolayer contents p_m/p_0 are between 0.1 and 0.15 according to the BET analysis. Figs. 3c–3e illustrate that the second adsorbed layer is only beginning to develop and negligible in a relative pressure of 0.1–0.15. Therefore, the monolayer capacity obtained via BET analysis is reliable if the sample meets the scope of BET.

Table 1 Validation data sets and calculated results.

Sample	Description	Data type	BET results					Data source
			m_m	C	S_{BET}	S_{GEO}	S	
			g/g		m^2/g	m^2/g	m^2/g	
a-quartz	Mineral	GCMC	0.103	45.7	359	296	295	Self-simulated
Mica	Mineral	GCMC	0.246	52.6	856	705	696	Self-simulated
Muscovite	Mineral	GCMC	0.125	37.1	435	354	355	Self-simulated
Kaolinite	Clay mineral	GCMC	0.378	35.4	1318	1075	1039	Self-simulated
Montmorillonite-Na	Clay mineral	GCMC	0.288	38.8	1003	769	804	Self-simulated
Montmorillonite-K	Clay mineral	GCMC	0.286	45.7	997	757	799	Self-simulated
S300K	Catalyst	GCMC	0.078	331.7	270	227	222	Herdes et al., 2011[26]
Carbon pore	Carbon	GCMC	0.098	31.5	342	261	268	Zou et.al, 2020[7]
MCM48	Catalyst	Measured	0.316	22.8	1098	892	918	Thommes et.al, 2000[27]
SBA15	Catalyst	Measured	0.203	974.7	707	600	583	Rocha et.al, 2021[28]
GA	Catalyst	Measured	0.076	317.9	264	227	225	Lidia et.al, 2021[8]
NP55	Catalyst	Measured	0.117	108.8	406	332	339	Lidia et.al, 2021[8]
NP38	Catalyst	Measured	0.067	335.2	232	184	197	Lidia et.al, 2021[8]
G10	Catalyst	Measured	0.082	187.3	284	224	241	Lidia et.al, 2021[8]
S383	Catalyst	Measured	0.232	114.8	809	665	675	Lidia et.al, 2021[8]
S403	Catalyst	Measured	0.180	214.1	626	510	533	Lidia et.al, 2021[8]
S383.HT	Catalyst	Measured	0.135	105.8	470	391	398	Lidia et.al, 2021[8]
S403.HT	Catalyst	Measured	0.135	80.0	470	378	391	Lidia et.al, 2021[8]

Note: m_m is monolayer content; C is an energetic parameter of BET analysis; S_{BET} is the surface area calculated by traditional BET analysis; S_{GEO} is the referenced geometric surface area; S is the surface area calculated by the proposed method.

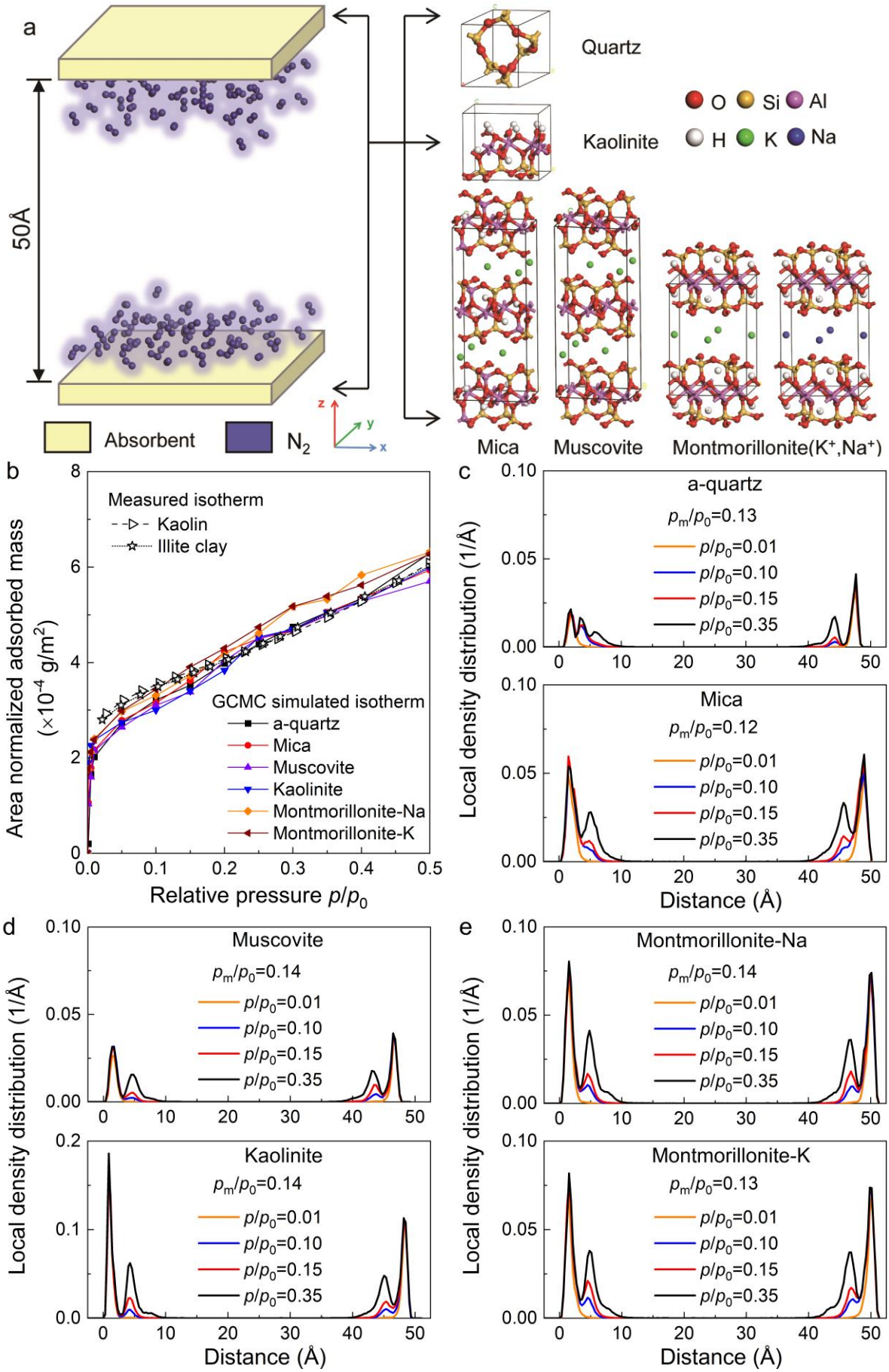

Fig. 3 Illustration of GCMC simulation and data processing. a Diagram of the GCMC model. **b** Nitrogen isotherm generated via the GCMC method and its comparison with the measured nitrogen isotherm. All isotherms are normalized on the surface area. **c** Local density distribution at a relative pressure of 0.01, 0.10, 0.15, and 0.35 for different minerals.

Both the traditional BET analysis and the proposed method are applied to all the nitrogen isotherms. The positive BET parameter C in all samples indicated that it meets the scope of the BET analysis. The surface area results of BET analysis S_{BET} and the proposed method S are listed in Table 1. Referenced geometric surface area values obtained using geometrical dimensions of GCMC models and argon adsorption isotherms are denoted S_{GEO} and also presented in Table 1. The relative error (Method, Eqs. 10 and 11) is selected as the evaluation index. As shown in Fig. 4, the surface area calculated using the proposed method is very close to the referenced geometric surface area. Relative errors of the proposed method range from −3% to 7%, and the absolute value of the relative error of 13 samples is smaller than 3%. Notably, the traditional BET analysis overestimates the surface area by 16% to 32%, with the majority higher than 20%. The excellent comparative evaluation results demonstrated that the surface area calculated via the proposed method can be regarded as the geometric surface area. This finding holds true for numerous types of mesoporous materials.

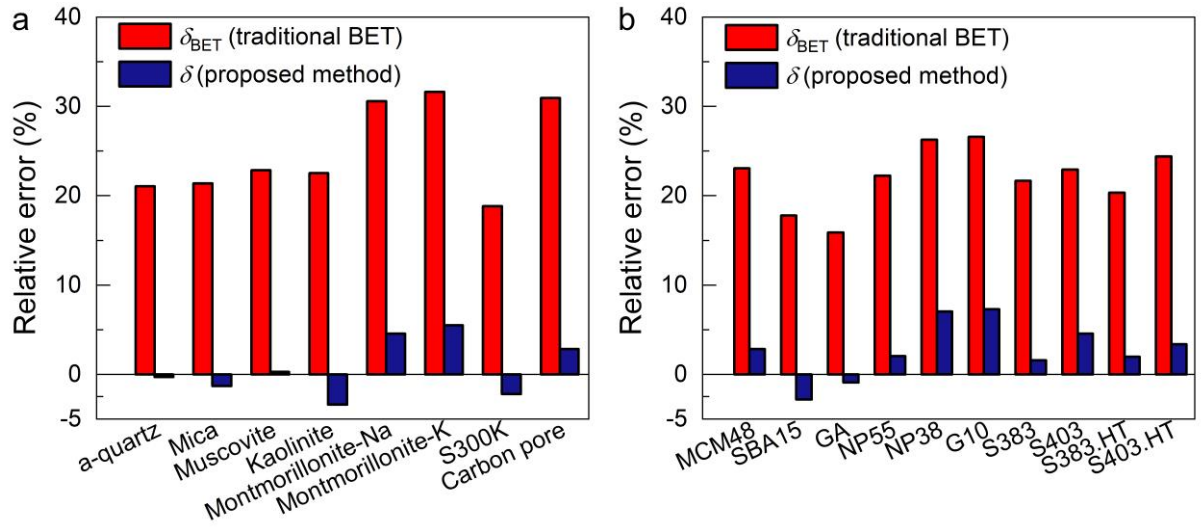

Fig. 4 Relative error between the referenced geometric surface area and the surface area calculated using the BET or proposed method. a Data are simulated using the GCMC method. **b** Data are experimentally measured.

Discussion

The BET equation has been typically used for surface area calculation. Our results showed that BET analysis performs properly on the monolayer content estimation of mesoporous materials. The overestimation of surface area from BET analysis is mainly due to the inappropriate cross-sectional area of the nitrogen molecule. The comparison of the BET and referenced geometric surface areas in Table 1 showed that the ratios of S_{BET} and S_{GEO} are varied for different samples. Hence, using a constant cross-sectional area is inappropriate. The proposed method fully considers the adsorption ability of different materials and can properly estimate the geometric surface area for a wide range of materials. Moreover, the proposed surface area calculation method can be widely applied because it only needs the nitrogen isotherm as the input. The generality, simplicity, and high accuracy jointly highlights the value of the proposed method.

Note that the density of the adsorbed phase obtained via the proposed method cannot be exactly the same as the actual state of the adsorbed nitrogen from the microscopic perspective. However, the surface area obtained using the proposed method can still be regarded as an excellent approximation of the geometric surface area. The comparison of results showed that our calculation can be generally and directly used as the geometric surface area.

Method

Gas adsorption experiment

Gas adsorption apparatuses have been widely used to measure the changes in pressure of pure calibrated gas, which is placed in a calibrated confined volume containing the measured adsorbent at a constant temperature[4]. If adsorption takes place, then the pressure in the confined volume decreases until equilibrium is reached. The adsorbed amount can be obtained according to the known amount of input adsorbate. The complete isotherm can then be constructed point by point by successively injecting the adsorbate. The experiment temperature is generally controlled by the temperature of the adsorbate in the liquid state under 0.1 MPa (e.g., 77 K for liquid nitrogen and 87 K for liquid argon). Isotherms utilized to validate the GCMC results (Fig. 3b) in this work were measured with a nitrogen adsorption apparatus (Nova 2000e, Quantachrome Instruments, USA).

Traditional BET analysis method

The BET equation is commonly used to calculate the monolayer content in the following linear form:

$$\frac{p / p_0}{(1 - p / p_0)m} = \frac{1}{Cm_m} + \frac{C - 1}{Cm_m} \times \frac{p}{p_0}, \quad (7)$$

where C is the parameter related to the sorption energy. The two unknown characteristic constants (m_m and C) can be easily obtained via linear regression of isotherm data. The relative pressure range recommended by the International Union of Pure and Applied Chemistry (IUPAC) BET analysis is 0.05–0.3[29], which is also the pressure range used in this study to obtain m_m.

Algorithm of geometric surface area calculation

The proposed algorithm for geometric surface area calculation consists of a start, 9 calculation steps, 3 decisions, and an end.

Input the isotherm data at the start stage. The isotherm provides the one-to-one relation between adsorbed mass and gas pressure, that is, $m= f(p)$ and $p=f^{-1}(m)$. Values within test data points are obtained via interpolation in this study.

The algorithm then comes into the preparation stage for surface area calculation. S1 (Step 1, similarly hereinafter): calculate m_m using Eq. 7. S2: initialize a temporally used surface area value S using Eq. 6 with m_m obtained in S1 and the density of bulk liquid nitrogen (0.81 g/cm^3).

The algorithm begins to calculate the adsorptive potential ψ_{ad} on the basis of the initialized S. S3 is a parameter setting step, where the density of bulk liquid nitrogen ρ_{bulk} also uses 0.81 g/cm^3. S4: the thickness of the adsorbed film is equal to 0.1 Å given that i =1. Hence, the total adsorbed mass is equal to m_{facial}, that is, the mass of bulk liquid nitrogen with the thickness of 0.1 Å. The corresponding gas pressure can then be solved with isotherm data, $p_1 = f^{-1}(m_1)$. ψ_{ad} at x=0.1 Å can be calculated using Eq. 5 and p_1. The algorithm then focuses on the next spatial location, that is, i = i+1. S5: the unknown adsorbed mass and corresponding gas pressure in this step are temporally calculated using $m_i = m_{i-1}+m_{facial}$ and $p_i = f^{-1}(m_i)$, respectively. The total potential ψ corresponding to m_i can be temporally calculated using Eq. 2 and p_i. S6: ψ_{ad} on the surface to x_{i-1} is known in this step. Therefore, the local pressure p_{ad} within the adsorbed phase on the surface to x_{i-1} can be calculated using Eq. 3, where ψ is obtained in S5. The local pressure controls the density of adsorbed phase using the following equation[19]:

$$\rho = -10^{-5} \times {p_{ad}}^2 + 0.0023 \times p_{ad} + 0.8078 \quad (8)$$

where p_{ad} is in MPa and ρ is in g/cm^3. If the local pressure is higher than 69 MPa, the upper limit pressure for liquid nitrogen[24], ρ takes the value of 1.1g/cm^3 [30]. The adsorbed mass can be updated using $m_i^{new} = m_{inner}+m_{facial}$, where m_{inner} is calculated by obtaining the sum of masses of all blocks between the surface and x_{i-1} on the basis of the density distribution of adsorbed phase. p_i^{new} =

348 $f^{-1}(m_i^{new})$ and obtain a new total potential ψ^{new} using Eq. 2 and p_i^{new}. If the difference between ψ^{new}
349 and the previously used ψ is smaller than 0.01 MPa, then proceed to S7; otherwise, replace ψ with
350 ψ^{new} and repeat S6 until the decision condition is satisfied. S7: calculate and record ψ_{ad} at x_i using
351 Eq. 5 and p_i. As shown in Figs. 3c–3e, 5 Å is significantly beyond the monolayer loading, which
352 is set as the upper limit for the ψ_{ad} calculation.

353 S9: the average density of the adsorbed phase at the state of monolayer loading can be
354 calculated on the basis of the determined adsorption potential ψ_{ad}. Note that the calculation of the
355 gas pressure p_m and thickness h of the adsorbed layer corresponding to the monolayer content is
356 simplified by interpolating m_i, p_i, and x_i data obtained from previous calculations. Calculate ψ
357 using p_m and Eq. 2. Calculate p_{ad} using ψ, ψ_{ad}, and Eq. 3. Calculate the local density distribution
358 using p_{ad} and Eq. 8. The average ρ_m^{ave} density of the monolayer can then be calculated using mass-
359 weighted average. Calculate the new surface area S^{new} using ρ_m^{ave} and Eq. 6. If the difference
360 between S^{new} and the initially used S is smaller than 0.01 m^2/g, then output the S value; otherwise,
361 replace S by S^{new} and repeat S4–S9.

362 **GCMC simulation**

363 Six typical mineral surfaces are selected for the molecular simulation. Among them, quartz is the
364 most important in the composition of sand. Kaolinite is the representative 1:1 clay mineral.
365 Muscovite, mica, and montmorillonite are selected as representative 2:1 clay minerals. The basic
366 structure and unit cell of these six minerals come from the Surface Model Database V1.5 of
367 INTERFACE[31,32] (Fig. 3a). A (5×3×1) supercell is created for each clay mineral surface to ensure
368 that the box length is larger than 10 times the collision diameter of nitrogen. A (6×6×4) supercell
369 is created for the quartz to obtain a similar dimension of the surface as that of clay minerals. A
370 surface plane is then formed by cleaving the supercell in the z-axis direction. Finally, a vacuum

layer with 50 Å is built on surfaces to ensure that only adsorption happens on two independent surfaces in the pressure range of the traditional BET analysis while avoiding the influence of both capillary condensation and periodic boundaries.

The GCMC method is utilized for isothermal adsorption of nitrogen on different kinds of minerals by means of Materials Studio. The simulation assumes a constant volume, temperature, and chemical potential within the system, while the number of nitrogen molecules is allowed to fluctuate. The simulation temperature of the system is 77 K. The chemical potential of nitrogen is associated with its pressure through an equation of state. The nitrogen adsorption isotherm is simulated by running a series of calculations at different pressure points from 0.1 kPa to 100 kPa. The van der Waals interaction between molecules is considered to represent the physical adsorption in the gas and mineral interface and calculated using Lennard–Jones (LJ) 9–6 equation[33-35].

$$E(r_{ij}) = \begin{cases} \varepsilon_0 \left[2\left(\frac{\sigma_0}{r_{ij}}\right)^9 - 3\left(\frac{\sigma_0}{r_{ij}}\right)^6 \right] & r_{ij} \le r_{\text{cutoff}} \\ 0 & r_{ij} > r_{\text{cutoff}} \end{cases}, \quad (9)$$

where r_{ij}, ε_0, and σ_0 are the respective separation, LJ well depth, and LJ radius between two atoms i and j, and r_{cutoff} is the cut-off distance in the LJ potential, which is 15.5 Å for clay minerals and 20 Å for quartz. Each Monte Carlo simulation consists of 1×10^6 steps for equilibrium and 1×10^6 steps for sampling. The average simulation results throughout the sampling stages are obtained.

Indexes for comparison

The relative error δ_{BET} and δ are used to evaluate the respective deviations between the surface area determined by the traditional BET analysis S_{BET} or the proposed method S and the referenced geometric surface area S_{GEO} as follows:

392 $$\delta_{\mathrm{BET}} = (S_{\mathrm{BET}} - S_{\mathrm{GEO}}) / S_{\mathrm{GEO}}, \quad (10)$$

393 $$\delta = \left(S - S_{\mathrm{GEO}}\right) / S_{\mathrm{GEO}}. \quad (11)$$

394

Data availability

The isotherm data generated in this study are provided within the paper.

Code availability

The code is available upon request.

Acknowledgements

This research is supported by the National Natural Science Foundation of China (51979144), the National Key Research and Development Program of China (2020YFC1806502), and the State Key Laboratory of Hydro-Science and Engineering (SKLHSE-2020-KY-01). Molecular simulation in this study is supported by the Center of High Performance Computing, Tsinghua University.

Author contributions

Y.W. conceived the research. L.H. supervised the research. Z.C. simulated the isotherms. Y.W. implemented the algorithm. All the authors analyzed the data and wrote the paper.

Competing interests

The authors declare no competing interests.

References

1 Leofanti, G., Padovan, M., Tozzola, G. & Venturelli, B. Surface area and pore texture of catalysts. *Catalysis Today* **41**, 207-219, doi:10.1016/s0920-5861(98)00050-9 (1998).

2 Heister, K. The measurement of the specific surface area of soils by gas and polar liquid adsorption methods—Limitations and potentials. *Geoderma* **216**, 75-87, doi:10.1016/j.geoderma.2013.10.015 (2014).

3 Peigney, A., Laurent, C., Flahaut, E., Bacsa, R. R. & Rousset, A. Specific surface area of carbon nanotubes and bundles of carbon nanotubes. *Carbon* **39**, 507-514, doi:10.1016/s0008-6223(00)00155-x (2001).

4 Thommes, M. *et al.* Physisorption of gases, with special reference to the evaluation of surface area and pore size distribution (IUPAC Technical Report). *Pure and Applied Chemistry* **87**, 1051-1069, doi:10.1515/pac-2014-1117 (2015).

5 Brunauer, S., Emmett, P. H. & Teller, E. Adsorption of gases in multimolecular layers. *J Am Chem Soc* **60**, 309-319, doi:DOI 10.1021/ja01269a023 (1938).

6 Sing, K. S. W. Adsorption methods for the characterization of porous materials. *Advances in Colloid and Interface Science* **76-77**, 3-11, doi:10.1016/s0001-8686(98)00038-4 (1998).

7 Zou, J., Fan, C. & Liu, X. Effects of Molecular Cross-Sectional Areas of Adsorbed Nitrogen on the Brunauer-Emmett-Teller Analysis for Carbon-Based Slit Pores. *Langmuir* **36**, 14656-14665, doi:10.1021/acs.langmuir.0c02514 (2020).

8 López-Pérez, L., Zarubina, V. & Melián-Cabrera, I. The Brunauer–Emmett–Teller model on alumino-silicate mesoporous materials. How far is it from the true surface area? *Microporous and Mesoporous Materials* **319**, 111065, doi:10.1016/j.micromeso.2021.111065 (2021).

9 Neimark, A. V., Kheifets, L. I. & Fenelonov, V. B. Theory of preparation of supported catalysts. *Industrial & Engineering Chemistry Product Research and Development* **20**, 439-450, doi:10.1021/i300003a006 (1981).

10 Gomez-Gualdron, D. A., Moghadam, P. Z., Hupp, J. T., Farha, O. K. & Snurr, R. Q. Application of Consistency Criteria To Calculate BET Areas of Micro- And Mesoporous Metal-Organic Frameworks. *J Am Chem Soc* **138**, 215-224, doi:10.1021/jacs.5b10266 (2016).

11 Leão, T. P. & Tuller, M. Relating soil specific surface area, water film thickness, and water vapor adsorption. *Water Resources Research* **50**, 7873-7885, doi:10.1002/2013wr014941 (2014).

12 Wang, J. & Hou, T. Develop and test a solvent accessible surface area-based model in conformational entropy calculations. *J Chem Inf Model* **52**, 1199-1212, doi:10.1021/ci300064d (2012).

13 Bafghi, M. S., Emami, A. H., Zakeri, A. & Khaki, J. V. Development and verification of a mathematical model for variations of the specific surface area of mineral powders during intensive milling. *Powder Technology* **197**, 87-90, doi:10.1016/j.powtec.2009.08.025 (2010).

14 Walton, K. S. & Snurr, R. Q. Applicability of the BET method for determining surface areas of microporous metal-organic frameworks. *J Am Chem Soc* **129**, 8552-8556, doi:10.1021/ja071174k (2007).

15 Yang, Q. *et al.* Capillary condensation under atomic-scale confinement. *Nature* **588**, 250-253, doi:10.1038/s41586-020-2978-1 (2020).

16 Fan, C., Zeng, Y., Do, D. D. & Nicholson, D. An undulation theory for condensation in open end slit pores: critical hysteresis temperature & critical hysteresis pore size. *Phys Chem Chem Phys* **16**, 12362-12373, doi:10.1039/c4cp00848k (2014).
17 Livingston, H. K. The cross-sectional areas of molecules adsorbed on solid surfaces. *Journal of Colloid Science* **4**, 447-458, doi:10.1016/0095-8522(49)90043-4 (1949).
18 Kodera, K. & Onishi, Y. The Molecular Cross-sectional Areas for the Determination of Specific Surface Areas of Solids. I. Carbon Black. *Bulletin of the Chemical Society of Japan* **32**, 356-361, doi:10.1246/bcsj.32.356 (1959).
19 Wang, Y., Hu, L., Zhang, C., Luo, S. & Lu, N. Liquid Cavitation during Nitrogen Sorption on Soils. *Journal of Engineering Mechanics* **147**, 04021099, doi:doi:10.1061/(ASCE)EM.1943-7889.0002008 (2021).
20 Gee, G. W., Campbell, M. D., Campbell, G. S. & Campbell, J. H. Rapid Measurement of Low Soil Water Potentials Using a Water Activity Meter. *Soil Science Society of America Journal* **56**, 1068-1070, doi:10.2136/sssaj1992.03615995005600040010x (1992).
21 Lu, N. & Zhang, C. Soil Sorptive Potential: Concept, Theory, and Verification. *Journal of Geotechnical and Geoenvironmental Engineering* **145**, 04019006, doi:10.1061/(asce)gt.1943-5606.0002025 (2019).
22 Israelachvili, J. N. *Intermolecular and surface forces*. (Academic press, 2011).
23 Tuller, M. & Or, D. Water films and scaling of soil characteristic curves at low water contents. *Water Resources Research* **41**, doi:10.1029/2005wr004142 (2005).
24 Span, R., Lemmon, E. W., Jacobsen, R. T., Wagner, W. & Yokozeki, A. A Reference Equation of State for the Thermodynamic Properties of Nitrogen for Temperatures from 63.151 to 1000 K and Pressures to 2200 MPa. *Journal of Physical and Chemical Reference Data* **29**, 1361-1433, doi:10.1063/1.1349047 (2000).
25 Zhang, C. & Lu, N. What Is the Range of Soil Water Density? Critical Reviews With a Unified Model. *Reviews of Geophysics* **56**, 532-562, doi:10.1029/2018rg000597 (2018).
26 Herdes, C., Russo, P. A., Carrott, M. M. L. R. & Carrott, P. J. M. Nitrogen Adsorption Studies on Non-Porous Silica: The Annealing Effect over Surface Non-Bridging Oxygen Atoms. *Adsorption Science & Technology* **29**, 357-364, doi:10.1260/0263-6174.29.4.357 (2011).
27 Thommes, M., Köhn, R. & Fröba, M. Sorption and Pore Condensation Behavior of Nitrogen, Argon, and Krypton in Mesoporous MCM-48 Silica Materials. *The Journal of Physical Chemistry B* **104**, 7932-7943, doi:10.1021/jp994133m (2000).
28 Villarroel-Rocha, J., Barrera, D., Arroyo-Gómez, J. J. & Sapag, K. Insights of adsorption isotherms with different gases at 77 K and their use to assess the BET area of nanoporous silica materials. *Adsorption* **27**, 1081-1093, doi:10.1007/s10450-021-00339-3 (2021).
29 Timmermann, E. O. Multilayer sorption parameters: BET or GAB values? *Colloids and Surfaces A: Physicochemical and Engineering Aspects* **220**, 235-260, doi:10.1016/s0927-7757(03)00059-1 (2003).
30 Cook, T. & Davey, G. The density and thermal conductivity of solid nitrogen and carbon dioxide. *Cryogenics* **16**, 363-369, doi:10.1016/0011-2275(76)90217-4 (1976).
31 Heinz, H., Lin, T. J., Mishra, R. K. & Emami, F. S. Thermodynamically consistent force fields for the assembly of inorganic, organic, and biological nanostructures: the INTERFACE force field. *Langmuir* **29**, 1754-1765, doi:10.1021/la3038846 (2013).
32 Chen, Z. & Hu, L. Adsorption of Naphthalene on Clay Minerals: A Molecular Dynamics Simulation Study. *Materials (Basel)* **15**, doi:10.3390/ma15155120 (2022).

33 Golzar, K., Amjad-Iranagh, S., Amani, M. & Modarress, H. Molecular simulation study of penetrant gas transport properties into the pure and nanosized silica particles filled polysulfone membranes. *Journal of Membrane Science* **451**, 117-134, doi:10.1016/j.memsci.2013.09.056 (2014).
34 Moradi, H., Azizpour, H., Bahmanyar, H. & Emamian, M. Molecular dynamic simulation of carbon dioxide, methane, and nitrogen adsorption on Faujasite zeolite. *Chinese Journal of Chemical Engineering* **43**, 70-76, doi:10.1016/j.cjche.2021.05.034 (2022).
35 Shi, J. *et al*. Competitive adsorption phenomenon in shale gas displacement processes. *RSC Adv* **9**, 25326-25335, doi:10.1039/c9ra04963k (2019).